



MANTA: Diffusion Mamba for Efficient and Effective Stochastic Long-Term Dense Anticipation

Olga Zatsarynna¹, Emad Bahrami¹, Yazan Abu Farha², Gianpiero Francesca³, Juergen Gall^{1,4}

¹University of Bonn, ²Birzeit University, ³Toyota Motor Europe, ⁴Lamarr Institute for Machine Learning and Artificial Intelligence

Abstract

Our work addresses the problem of stochastic long-term dense anticipation. The goal of this task is to predict actions and their durations several minutes into the future based on provided video observations. Anticipation over extended horizons introduces high uncertainty, as a single observation can lead to multiple plausible future outcomes. To address this uncertainty, stochastic models are designed to predict several potential future action sequences. Recent work has further proposed to incorporate uncertainty modelling for observed frames by simultaneously predicting per-frame past and future actions in a unified manner. While such joint modelling of actions is beneficial, it requires long-range temporal capabilities to connect events across distant past and future time points. However, the previous work struggles to achieve such a long-range understanding due to its limited and/or sparse receptive field. To alleviate this issue, we propose a novel MANTA (MAMBA for ANTicipation) network. Our model enables effective long-term temporal modelling even for very long sequences while maintaining linear complexity in sequence length. We demonstrate that our approach achieves state-of-the-art results on three datasets—Breakfast, 50Salads, and Assembly101—while also significantly improving computational and memory efficiency.

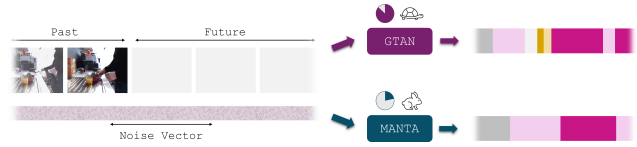


Figure 1. We propose a novel generator MANTA that allows for more efficient and effective stochastic long-term anticipation compared to the previous work.

multiple predictions for a single video observation are made to account for the uncertainty of future forecasting. Early works in this area [7, 60] predicted future action sequences based on a fixed set of pre-classified or ground-truth observed actions. Recently, GTDA [55] highlighted the limitations of this approach and proposed to model frame-wise past and future actions jointly with a single diffusion model, conditioned on the observed frames padded with zeros in place of future entries. To account for the differences between the observed and masked parts of the sequence, they introduced a GTAN diffusion generator - a multi-stage architecture of dilated temporal convolutional layers with data-dependent temporal gates.

Although their model demonstrated strong performance on the task of stochastic long-term anticipation, the proposed GTAN generator has certain limitations. Firstly, in the early layers of each stage, convolutional kernels have local support due to the small dilation factor. However, given the input structure, where observed frames are followed by masking values, the limited receptive field prevents padded values from accessing observed context and thus updating future frame values. While the multi-stage architecture partially mitigates this, it introduces additional parameters and increases computation. Moreover, while in the later layers, the dilation rate increases the receptive field, it remains sparse due to the small kernel size, with each sequence element accessing only a limited set of other elements, making updates highly restrictive. These limitations are particularly pronounced for longer videos with extended anticipation horizons, where the future-padded part of the input sequence becomes challenging to process.

To address these limitations, we propose a novel

1. Introduction

In this work, we address the task of stochastic long-term dense anticipation. This task focuses on forecasting actions and their durations over minutes-long future horizons. The length of the anticipation horizon and the need to predict the duration of future actions make this task particularly challenging. However, solving it is essential for many real-world applications, including autonomous driving and assembly line automation.

In our work, we focus on stochastic anticipation, where

¹Corresponding author: zatsarynna@iai.uni-bonn.de

MANTA (Mamba for ANTicipation) generator network, which incorporates the recently proposed Mamba layer [13] as its temporal processing block. Our resulting model maintains a global receptive field while keeping linear complexity relative to the sequence length, enabling early propagation of observed information across the entire masked area of the input sequence. This eliminates the need for a multi-stage architecture and reduces computational and memory costs. Additionally, our model maintains the ability to adaptively handle the two distinct parts of the input sequence - past observed frames and future masked frames - due to the inherent data-dependent gating mechanism.

We evaluate our proposed model on three challenging datasets: Breakfast [24], 50Salads [50], and Assembly101 [42]. Our results demonstrate state-of-the-art performance across all three of them. Furthermore, we show, that our model is significantly faster than the previous best-performing GTDA [55] model, achieving inference and training time speed-up of up to $65.3\times$ and $6.6\times$, respectively.

2. Related Work

Action Anticipation in Videos. Action anticipation has been explored in various works across different settings. Although the overarching goal remains to predict future actions based on observed video data, the key distinction lies in the temporal horizon of anticipation. On one hand, short-term anticipation approaches [10, 57, 56, 58, 8, 63, 29, 62, 43, 16, 40, 9] focus on predicting a single action a few seconds before it occurs. Long-term anticipation methods, on the other hand, aim to predict multiple future actions, resulting in forecasting horizons that span one or several minutes. Here, we focus on the latter setting.

In the context of long-term anticipation, several distinct settings exist that differ in their final prediction objectives. The focus of this work is *dense long-term anticipation*. Unlike different research directions that frame anticipation as ordered [12, 33, 3, 6, 61, 34] or unordered [37, 36, 64, 61] duration-agnostic transcript prediction problem, dense anticipation requires future actions to be predicted for a pre-defined number of future frames. This involves the estimation of both the order of actions and their durations. Dense long-term anticipation is further subdivided into deterministic and stochastic anticipation. Deterministic models [11, 1, 2, 55, 64, 43, 23] produce a single prediction for each video observation, while stochastic methods [7, 55, 64, 60] generate several plausible samples for each observation. In this work, we propose a stochastic long-term dense anticipation approach.

Farha *et al.* [7] introduced the first stochastic approach for dense anticipation by extending a deterministic RNN-based method [2] to predict multiple samples. Zhao *et al.* [60] enhanced the plausibility and diversity of these

predictions through adversarial learning. Instead of relying on pre-classified or ground-truth actions like previous approaches, recent methods [55, 64] perform past classification and future forecasting simultaneously. Zhong *et al.* [64] expanded the FUTR [11] decoder with diffusion [46, 48, 20, 49, 39] to model uncertainty in future actions. Zatsarynna *et al.* [55] proposed a gated temporal diffusion network to simultaneously model uncertainty in past and future actions, outperforming previous methods.

State-Space Models. Recent developments in sequence modeling have introduced efficient alternatives to attention-based architectures, such as State Space Models [14, 45, 15], which offer linear scaling with sequence length. Building on these approaches, Mamba [13] enhances the framework by introducing selective state space modeling with an input-dependent selection mechanism. Given Mamba’s potential for efficient modeling of long sequences, it has been adapted for tasks such as image classification [30, 65, 26], video understanding [25, 52, 26], medical imaging [32, 41, 53], image restoration [17], motion generation [59] and point cloud analysis [27]. Architectures based on state space models such as Mamba have recently been used as backbones for diffusion models in image and video generation [22, 35, 54]. In this work, distinct from previous studies, we focus on designing a Mamba-based model for both efficient and effective stochastic long-term action anticipation.

3. Method

To effectively handle the inherent uncertainties in action forecasting, we explore stochastic long-term anticipation, where models predict multiple possible future outcomes based on a single set of observed frames. Given the observed frames, these approaches learn to sample from the probability distribution of future action variables. Formally:

$$\tilde{\mathcal{Y}}^{P+1:P+F} \sim P(\mathcal{Y}^{P+1:P+F} | g(x_1) : g(x_P)), \quad (1)$$

where g is a feature extractor, x_i is the i^{th} video frame, \mathcal{Y}^i is the variable corresponding to frame i , and $\tilde{\mathcal{Y}}^i$ is a sample from \mathcal{Y}^i ; P and F represent the number of past and future frames, respectively. Recently, Zatsarynna *et al.* [55] proposed to jointly model the uncertainty of actions in both observed and future frames using a common diffusion model. In this way, they modelled a more general distribution - the joint observation-conditioned probability of both observed and future actions. That is:

$$\tilde{\mathcal{Y}}^{1:P+F} \sim P(\mathcal{Y}^{1:P+F} | g(x_1) : g(x_P)). \quad (2)$$

This allowed their diffusion to model actions in the future and past frames in a consistent manner. Furthermore, to take into account distinctions between these two types of variables, they proposed a GTAN diffusion generator network,

that employed gated dilated temporal convolutional layers to process the sequence with data-dependent gates. The use of dilated convolutions for temporal processing, however, poses several limitations. Specifically, the exponentially increasing dilation rates (2^{l-1}) of the convolutional kernels result in limited receptive fields in the early layers and sparse receptive fields lacking local context in the later layers. This leads to two issues: the limited receptive field of early layers prevents observed information from reaching future masked entries, while the large, sparse receptive fields of the later layers restrict updates and lack local awareness. Although the multi-stage design intends to address these issues, it only partially mitigates them, while adding to computational and memory costs.

In this work, we address the limitations mentioned above. While we follow Zatsarynna *et al.* [55] in harnessing the unified diffusion process for observed and future action modelling, we introduce a novel MANTA generator model. By utilizing the Mamba [13]-based layers, our model sustains a global receptive field across the entire network while preserving local awareness. Additionally, relying on the data-dependent gating our model processes the input sequence adaptively, considering the difference between its two components - observed and future actions. In the following sections, we present the details of our proposed model. In Sec. 3.1, we describe how the diffusion process is formulated for addressing the task of stochastic long-term dense anticipation. Then, in Sec. 3.2, we present the details of our proposed MANTA model.

3.1. Diffusion for Long-Term Dense Anticipation

General Diffusion. Diffusion models are generative models that learn to produce samples from data distributions by reconstructing progressively noisier versions of data points. To achieve this, two Markov chain processes are defined: the *forward* and the *reverse*. The forward Markov process $q(\mathcal{Y}_t|\mathcal{Y}_{t-1})$ defines the transition from the data distribution to Gaussian noise, using a predefined noising schedule. In contrast, the reverse Markov process $p_\theta(\mathcal{Y}_{t-1}|\mathcal{Y}_t)$ models the inverse transition, from random noise back to the data distribution.

The reverse process is parameterized by a diffusion generator network \mathcal{G}_θ that is trained to reconstruct data points corrupted by the forward process: $\tilde{\mathcal{Y}}_{0,t} = \mathcal{G}_\theta(\mathcal{Y}_t, t)$. Here, \mathcal{Y}_t is the corrupted data sample and $\tilde{\mathcal{Y}}_{0,t}$ is the reconstructed data point.

Anticipation Diffusion. We follow the formulation of diffusion anticipation model proposed in [55]. Following Eq. (2), anticipation diffusion reconstructs one-hot encoded per-frame past and future ground-truth actions conditioned on the padded visual features of observed frames. More specifically, the diffusion latent variables \mathcal{Y}_t are introduced to model per-frame actions, with a total of $(P + F)$ vari-

ables. To condition anticipation on past video frames, latent variables \mathcal{Y}_t are concatenated with a vector \mathcal{X} , constructed by extending observed visual features with zeros in place of future action variables to account for the corresponding unobservable visual features:

$$\mathcal{X} = \{g(x_1), \dots, g(x_P), \underbrace{0, \dots, 0}_F\}, \quad (3)$$

In this way, the future reconstruction is computed as $\mathcal{G}_\theta(\mathcal{Y}_t, t, \mathcal{X})$. Next, we provide a detailed description of our proposed MANTA generator \mathcal{G}_θ .

3.2. Model

The overview of our proposed MANTA model is shown in Fig. 2. The key contribution of our model is the Bidirectional Selective State-Space Layer (BSSL), which enables effective and efficient long-range temporal modelling and supports selective sequence processing through data-dependent gating. These properties are essential for long-term dense anticipation, where framewise prediction of past and future actions requires reasoning over lengthy sequences with a structured pattern: observed frames followed by masked future frames. Next, we describe our proposed BSS layer in Sec. 3.2.2, after detailing deep state-space models in Sec. 3.2.1, which serve as its foundation. We then discuss the overall structure of our proposed MANTA model in Sec. 3.2.3.

3.2.1 Deep Structured State-Space Models

Deep structured state-space models (SSMs) are a recently developed class of sequence models, inspired by continuous linear time-invariant state-space models, that define a mapping from an input sequence $x(t) \in \mathbb{R}$ to an output sequence $y(t) \in \mathbb{R}$ through a latent state $h(t) \in \mathbb{R}^N$ using a first-order ordinary differential equation:

$$h'(t) = \mathbf{A}h(t-1) + \mathbf{B}x(t), \quad (4)$$

$$y(t) = \mathbf{C}h(t), \quad (5)$$

where $\mathbf{A} \in \mathbb{R}^{N \times N}$, $\mathbf{B} \in \mathbb{R}^{N \times 1}$ and $\mathbf{C} \in \mathbb{R}^{N \times 1}$ are state, input and output matrices, respectively. Deep SSMs are defined by transforming the above formulation into a discrete-time learnable system. To this end, continuous-time equations (4) and (5) are discretized with a time-step parameter Δ .

$$h_t = \bar{\mathbf{A}}h_{t-1} + \bar{\mathbf{B}}x_t, \quad (6)$$

$$y_t = \mathbf{C}h_t, \quad (7)$$

$$\bar{\mathbf{A}} = \exp(\Delta\mathbf{A}), \quad (8)$$

$$\bar{\mathbf{B}} = \exp(\Delta\mathbf{A})^{-1}(\exp(\Delta\mathbf{A}) - I)\Delta\mathbf{B}. \quad (9)$$

These discretized equations form the foundation for a class of deep SSMs *S4* [14], which define a sequence-to-sequence

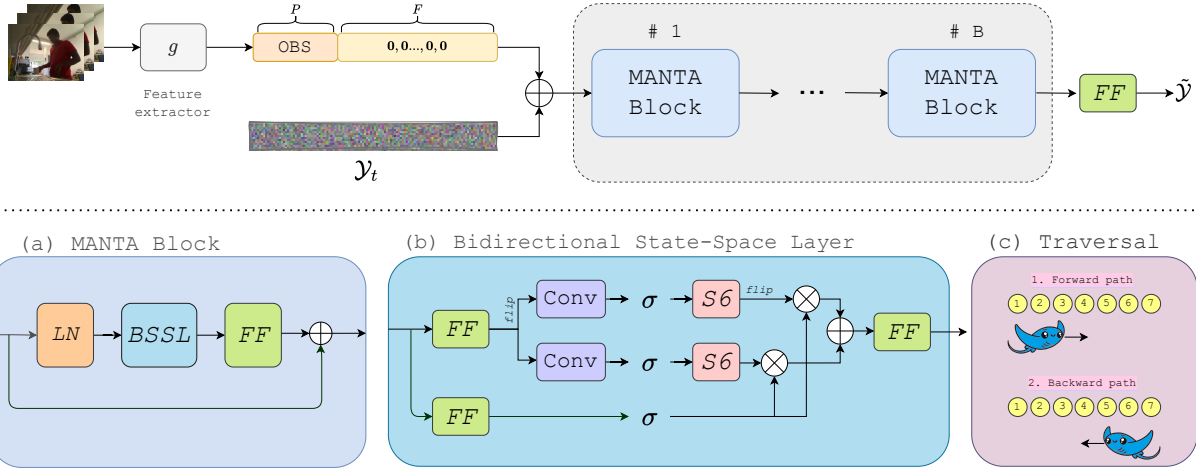


Figure 2. (Top) Overview of the proposed MANTA model. (Bottom) Illustration of the structure of the (a) MANTA block, (b) Bidirectional State-Space Layer, as well as (c) traversal directions of the BSSL for the temporal input sequence.

transformation parametrized by a set of learnable parameters (\mathbf{A} , \mathbf{B} , \mathbf{C} , and Δ) following Eq. (6) and (7). To compute this model, its parameters are transformed into $(\bar{\mathbf{A}}, \bar{\mathbf{B}})$ using Eq. (8) and (9), after which output y is acquired either via linear recurrence or global convolution.

While $S4$ models maintain a global receptive field, they do not implement selective value processing, since the parameters (\mathbf{A} , \mathbf{B} , \mathbf{C} , and Δ) remain fixed over time. Recently, Gu *et al.* [13] proposed an improved $S6$ layer by introducing the selection mechanism into the $S4$ model. To this end, they proposed to make parameters input-dependent by computing them as functions of $x \in \mathbb{R}^{B \times T \times D}$, i.e. $\mathbf{B}(x) \in \mathbb{R}^{B \times T \times N}$, $\mathbf{C}(x) \in \mathbb{R}^{B \times T \times N}$, and $\Delta(x) \in \mathbb{R}^{B \times T \times D}$. This increases the model’s adaptability, enabling data-driven information selection from both hidden states h_t and input sequence entries x_t . While it also leads to increased capacity, the output of $S6$ model can be efficiently computed using a parallel-scan algorithm.

The tradeoff between keeping and pruning the information in the input and hidden vectors is controlled by the parameters of $S6$, which can be interpreted to have specific functions within the model, as described in [13, 18]. On one hand, Δ can be viewed as an *input gate*, controlling how much information from the input x_t gets propagated into the hidden state h_t . Conversely, $\bar{\mathbf{A}}$ functions as a *forget gate*, determining the extent of pruning of the previous hidden state h_{t-1} . Finally, \mathbf{C} controls how much information from h_t propagates into the output y_t . In this way, the data-dependent gating of the $S6$ adopts a similar role as the gated convolution of the GTAN, which adjusts the output of temporal convolutional layers using temporal gates.

3.2.2 Bidirectional State-Space Layer

For BSSL, we make use of the above-described $S6$ layer as our temporal processing unit, due to its attractive properties of maintaining locally-aware [18] global receptive field, in contrast to GTAN, whose receptive field is limited by the dilation factor of the convolution layers. Apart from that, the selective modelling of the input sequence based on the data-dependent gating of the underlying SSM model is a crucial property which enables MANTA to perform anticipation effectively.

We base our layer on the Mamba block, proposed in [13], which incorporates the $S6$ layer into the residual block for efficient and effective sequence processing. The general overview of the BSSL’s structure is depicted in Fig. 2(b). Following [13], our proposed layer consists of two branches: the main branch (top) and the residual branch (bottom). The residual branch implements a multiplicative residual connection within the layer. Specifically, it uses a linear projection layer to map the input feature F_t^b to a space with 2-times expanded channels, followed by the activation function σ (SiLU [19, 38]), resulting in the vector R_t^b :

$$R_t^b = \sigma(FF(F_t^b)) \quad (10)$$

The main branch consists of two sub-branches: forward and backward. While the original Mamba block processes the input sequence solely in a forward direction, several recent works [25, 65, 30] have demonstrated the sub-optimality of this approach for visual sequences due to a lack of temporal awareness. To address this issue, following [25], we extend the main branch with an additional backward pass to process the input sequence in reverse order (Fig. 2(c)). We analyzed the benefit of this extension in Sec. 4.5.

As shown in Fig. 2(b), the forward and backward paths are applied to the linearly projected input sequence sepa-

rately. Both paths follow the same flow: after a depth-wise convolution, the input is processed by the $S6$ layer, whose output is then activated by σ . After that, a residual connection is applied to the outputs of both paths independently. Importantly, before and after processing the sequence with the backward path, it is flipped in time. Formally:

$$W_t^b = S6(\sigma(H^K * FF(F_t^b))), \quad (11)$$

$$B_t^b = S6(\sigma(H^K * FF(\overleftarrow{F_t^b}))), \quad (12)$$

$$W_t^b = W_t^b \odot R_t^b, \quad B_t^b = \overleftarrow{B_t^b} \odot R_t^b, \quad (13)$$

Here H^K is a 1D convolutional filter with size K , flipping across temporal dimension is denoted as $\overleftarrow{\cdot}$, while $*$ and \odot are convolution and element-wise multiplication, respectively. The output feature of the BSSL block is computed by accumulating the outputs of backward and forward paths as follows:

$$O_t^b = FF(W_t^b + B_t^b). \quad (14)$$

3.2.3 MANTA

Depicted in Fig. 2 (top), our proposed network consists of B MANTA blocks that process the input to predict future actions. Given pre-extracted observed frame features, we first pad them with zeros in place of future frames as described in Eq. (3), creating a conditioning vector $\mathcal{X} \in \mathbb{R}^{(P+F) \times n_d}$. \mathcal{X} is then concatenated with latent variables \mathcal{Y}_t along the channel dimension to form $F_t \in \mathbb{R}^{(P+F) \times (n_c + n_d)}$, which is sequentially processed by MANTA blocks to generate the output feature \tilde{F}_t , based on which the final prediction $\tilde{\mathcal{Y}}_{0,t} \in \mathbb{R}^{(P+F) \times n_c}$ is made using an MLP layer. Here n_c and n_d denote number of classes and number of feature channels, respectively.

The structure of individual MANTA blocks follows the design shown in Fig. 2(a). For block b , its input feature F_t^b is first normalized using Layer Normalization (LN) [4] and then passed through a BSSL, which performs temporal modelling of the input. Finally, a channel-mixing feed-forward layer is applied, followed by a residual connection. In summary, we can express the block’s operation in the following way:

$$F_t^{b+1} = FF(BSSL(LN(F_t^b))) + F_t^b. \quad (15)$$

3.2.4 Training and Inference

For training our proposed MANTA model, we follow the established diffusion training approach [20]. Given a step t sampled uniformly at random, we obtain \mathcal{Y}_t using the forward diffusion process. We then pass \mathcal{Y}_t alongside the conditioning vector \mathcal{X} to our proposed MANTA model to obtain reconstruction $\tilde{\mathcal{Y}}_{0,t}$ of the ground-truth action sequence

\mathcal{Y}_0 . Finally, we compute the \mathcal{L}_2 -loss between the predicted and the one-hot-encoded ground-truth action sequences:

$$\mathcal{L}_{rec} = \mathbb{E}_{\mathcal{Y}_{0,t}, \epsilon_t} \|\mathcal{Y}_0 - \tilde{\mathcal{Y}}_{0,t}\|^2. \quad (16)$$

During inference, we generate multiple predictions (S) for a single set of observed frames \mathcal{X} . To do so, we sample multiple start noise vectors $\{\mathcal{Y}_{T,s}\}_{s=1}^S \sim \mathcal{N}(\mathbf{0}, \mathbf{I})$, which we subsequently denoise using our proposed MANTA model to obtain $\{\tilde{\mathcal{Y}}_{0,1,s}\}_{s=1}^S$. To shorten the inference time, following [55], we employ the DDIM [47] sampling method and take $D < T$ out of T diffusion steps.

4. Experiments

4.1. Datasets

To evaluate our proposed model, we use three datasets commonly utilized for stochastic long-term anticipation tasks: Breakfast [24], Assembly101 [42] and 50Salads [50]. **Breakfast** [24] is a dataset of cooking videos in which human actors prepare 10 different breakfast meals in various kitchen environments. It comprises 1,712 videos that are densely annotated with temporal segments across 48 action classes. The dataset includes videos of varying durations, with the longest sequence lasting 10.8 minutes, which requires an anticipation horizon of up to 5.4 minutes. Following previous work, we evaluate our model using 4 predefined cross-validation splits and report the mean performance across these splits.

Assembly101 [42] is a large-scale dataset of toy assembly and disassembly videos captured from multiple exocentric and egocentric viewpoints, comprising a total of 4,321 videos. The video sequences are densely annotated with temporal action segments from 202 coarse action classes. The longest video duration for Assembly101 is over 25 minutes, requiring anticipation up to 12.5 minutes into the future. Following prior work [55], we train our network on the training split and report evaluation results on the validation set, as the test set is not publicly available.

50Salads [50] is a dataset of salad preparation videos, consisting of 50 video sequences annotated with dense temporal segments from 17 action classes. The mean video duration is 6.4 minutes, with the longest video sequence lasting 10.1 minutes, which requires an anticipation horizon of up to 5.1 minutes. For evaluation, we report the performance of our model averaged over the 5 standard predefined cross-validation splits.

4.2. Implementation Details

Following previous methods, we make use of the same pre-extracted frame features. Specifically, we use I3D features from [1, 11] for the Breakfast and 50Salads datasets, while for Assembly101 we rely on TSM-features [28] provided by [42]. Additionally, to ensure a fair comparison

MoC	Method	$\beta (\alpha = 0.2)$				$\beta (\alpha = 0.3)$			
		0.1	0.2	0.3	0.5	0.1	0.2	0.3	0.5
Breakfast									
Mean	Tri-gram [7]	15.4	13.7	12.9	11.9	19.3	16.6	15.8	13.9
	UAAA [7]	15.7	14.0	13.3	13.0	19.1	17.2	17.4	15.0
	DiffAnt [64]	24.7	22.9	22.1	22.3	30.9	30.2	28.9	27.5
	GTDA [55]	24.0	22.0	21.4	20.6	29.1	26.8	25.3	24.2
	Ours	27.7	25.3	24.6	23.8	34.2	30.9	29.1	27.7
Top-1	Tri-gram [7]	-	-	-	-	-	-	-	-
	UAAA [7]	28.9	28.4	27.6	28.0	32.4	31.6	32.8	30.8
	DiffAnt [64]	31.3	29.8	29.4	30.1	37.4	37.0	36.3	34.8
	GTDA [55]	51.2	47.3	45.6	45.0	54.0	50.4	49.6	47.8
	Ours	55.5	51.0	47.9	46.9	59.6	55.0	53.7	51.9
Assembly101									
Mean	Tri-gram [55]	2.8	2.2	1.9	1.5	3.5	2.7	2.3	1.8
	UAAA [7]	2.7	2.1	1.9	1.7	2.4	2.1	1.9	1.7
	GTDA [55]	6.4	4.5	3.5	2.8	5.9	4.2	3.5	2.9
	Ours	6.7	5.3	4.2	3.5	6.6	4.7	4.2	3.5
	Top-1	Tri-gram [55]	9.0	8.0	7.2	5.6	9.5	8.2	7.8
UAAA* [7]		6.9	5.9	5.6	5.1	5.9	5.5	5.2	4.9
GTDA [55]		18.0	12.8	9.9	7.7	16.0	11.9	10.2	7.7
Ours		16.9	13.3	10.2	8.8	15.6	12.0	11.1	8.4
50Salads									
Mean	Tri-gram [7]	21.4	16.4	13.3	9.4	24.6	15.6	11.7	8.6
	UAAA [7]	23.6	19.5	18.0	12.8	28.0	18.0	14.8	12.1
	GTDA [55]	28.3	22.1	17.8	11.7	29.9	18.5	14.2	10.6
	Ours	28.6	22.8	19.5	13.6	31.3	21.9	17.6	13.0
	Top-1	Tri-gram [7]	-	-	-	-	-	-	-
UAAA* [7]		53.5	43.0	40.5	33.7	56.4	42.8	35.8	30.2
GTDA [55]		69.6	55.8	45.2	28.1	66.2	44.9	39.2	31.0
Ours		68.3	51.5	41.7	31.3	71.7	53.3	43.8	31.1

Table 1. Comparison of MANTA to the state-of-the-art methods on Breakfast, Assembly101 and 50Salads.

with [55], we closely follow their implementation. We provide further details in the supp. mat.

4.3. Protocol and Evaluation

In this work, we adopt the stochastic long-term dense anticipation protocol proposed by Farha *et al.* [7]. In this setting, the observation length and anticipation horizon are defined relative to the video duration. Specifically, for a video v with n_v total frames, the model observes $P = \alpha n_v$ frames and then anticipates action labels for the subsequent $F = \beta n_v$ frames, where α and β represent the observation and anticipation percentages.

For evaluation, we also closely follow prior work [55, 7]. Specifically, for each observed video snippet, we sample $S = 25$ predictions from our model. As our evaluation metrics, we report Mean and Top-1 MoC (Mean over Classes) accuracy: Mean MoC measures the average MoC across the S generated samples, while Top-1 MoC reflects the MoC of the best-matching sample. Consistent with previous works, we report the results for $\alpha \in \{0.2, 0.3\}$ and $\beta \in \{0.1, 0.2, 0.3, 0.5\}$.

4.4. Results

Comparison to the State of the Art. In this section, we present the results of our proposed model, comparing



Figure 3. Qualitative comparison on MANTA and GTDA on Breakfast. Best viewed zoomed in.

its performance with the previous methods, as shown in Tab. 1. Our model achieves state-of-the-art results across all three datasets for both reported metrics. Specifically, on the Breakfast dataset, our method significantly outperforms previous approaches across all observation and anticipation horizons. On the Assembly101 dataset, MANTA surpasses all prior methods, with the exception of Top-1 MoC accuracy for $\beta = 0.1$, where it performs on par with GTDA. Lastly, on the 50Salads dataset, our approach sets a new state-of-the-art for Mean MoC accuracy and Top-1 MoC accuracy for $\alpha = 0.3$. For $\alpha = 0.2$, our model’s Top-1 MoC is on par with earlier methods.

Beyond its effectiveness, our proposed model demonstrates substantial efficiency improvements compared to [55]. Fig. 4 compares the inference and training time of MANTA and the previous best-performing method GTDA [55] on the Breakfast dataset. On the left, it shows the average inference time required to generate $S = 25$ samples with observation and anticipation ratios set to $\alpha = 0.3$ and $\beta = 0.5$ for videos in the test splits. While GTDA requires an average of 71.8 seconds per video, our model needs only 1.1 seconds, achieving a $65.3\times$ speedup. Besides faster inference, our model significantly reduces training time as well, as shown in Fig. 4 on the right. The average runtime for a single epoch of GTDA is 379 seconds, while MANTA only takes 57 seconds per epoch. Additionally, due to the reduced number of the required blocks, our proposed model has $2.8\times$ fewer parameters compared to GTDA, as shown in Tab. 6 and is therefore much more memory-efficient.

Finally, we demonstrate a qualitative comparison of our model to GTDA in Fig. 3. While GTDA anticipates future actions wrong, our proposed MANTA model predicts plausible action sequences. This demonstrates the limitations of the previous generator compared to our model, caused by its sparse receptive field lacking global context, leading not only to faulty predictions but also to over-segmentation.

4.5. Ablations

In this section, we discuss a series of experiments that we performed to explore individual components of our proposed MANTA model. Further ablations experiments are provided in the supp. mat.

Bidirectional State-Space Layer. The key component of MANTA is the BSS layer, discussed in Sec. 3.2.2. We conducted a series of experiments to investigate how different formulations of this layer affect the proposed model.

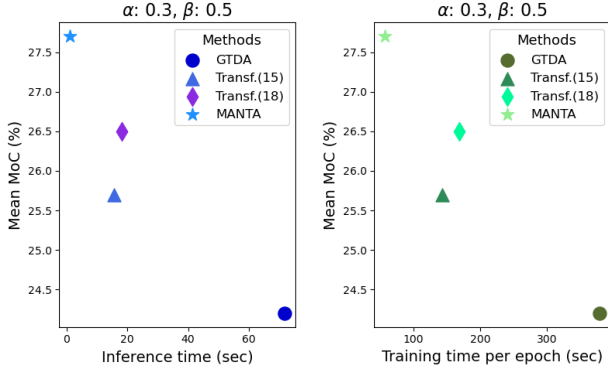


Figure 4. (Left) Mean time for generating 25 samples measured for different models on Breakfast, with all models performing 50 inference diffusion steps; (Right) Mean time required for training different models for one epoch on Breakfast. (Both) The batch size is equal across models, and evaluation/training was conducted on the same GPU.

Specifically, we examine how the following properties contribute: *selectivity* and *bi-directionality*.

Firstly, the *selectivity* of the BSS layer is enabled by employing the *S6* layer for temporal modelling, which applies input-specific SSM matrices for data-driven sequence processing. To assess the impact of selectivity, we replaced the *S6* layer with *S4*, for which the parameters remain fixed across timesteps. The results in Tab. 2 show a significant performance drop without selectivity (Ours w/o Sel.). This is expected, as the input sequences to our model consist of two distinct segments: observed and masked future frames. Processing these segments homogeneously is inherently sub-optimal, since it is not possible to adjust the contribution of individual values regardless of their validity and/or importance. GTDA made similar observations, where selectivity was ensured by data-driven temporal gating.

Secondly, we investigated the impact of *bi-directionality* in the BSSL, which processes the input sequence from both ends using forward and backward branches (Fig. 2(b) and (c)). To assess the role of the backward branch, we tested two models where the backward path was removed. First, we removed it from the first 10 MANTA blocks, leaving only the last 5 bidirectional blocks, and then removed it entirely, resulting in 0 bidirectional blocks. The results in Tab. 3 show a performance drop in both cases, with the performance of the fully uni-directional network particularly

MoC	BSSL type	$\beta(\alpha = 0.2)$				$\beta(\alpha = 0.3)$			
		0.1	0.2	0.3	0.5	0.1	0.2	0.3	0.5
Mean	Ours w/o Sel.	26.4	24.4	23.5	23.2	31.7	28.9	27.3	26.5
	Ours w/ Sel.	27.7	25.3	24.6	23.8	34.2	30.9	29.1	27.7
Top-1	Ours w/o Sel.	47.3	44.5	41.9	41.8	51.6	47.5	46.3	44.6
	Ours w/ Sel.	55.5	51.0	47.9	46.9	59.6	55.0	53.7	51.9

Table 2. Ablation of the selectivity of the BSSL layer on Breakfast.

affected. This suggests that the backward flow of information is crucial for model performance, highlighting the importance of sequence processing in both directions.

MANTA Block. We further performed a series of experiments to explore how changes to the MANTA Block beyond the BSSL affect the performance of the final model. Firstly, we investigated the effect of the internal structure of the block, as shown in Tab. 4. We experimented with introducing a dilated convolution layer with an exponentially growing dilation rate (Ours w/ Dil. Conv) before the LN layer, akin to [55]. This, however, led to the degradation of results. Moreover, following recent works [17, 44], we experimented with modifying the channel mixing (FF) component of our block. Removing the mixing MLP altogether (Ours w/o FF) hinders the performance, as expected, due to a lack of channel-wise communication. However, introducing channel attention (Ours w/ SE), as proposed in [17], fails to improve the results and leads to a performance drop. Finally, we experimented with varying the total number of blocks in the final model (Tab. 5). Empirically, we found that the model with $B = 15$ blocks showed the best results, with further increase or decrease in the number of blocks harming the model’s performance.

Attention. To better understand the benefits of the proposed model, particularly the state-space model-based MANTA block, we explored the alternative of utilizing the attention-based Transformer (Transf.) [51] block instead. Like SSM-based models, transformers have a global tem-

MoC	Blocks w/ Fwd.	Blocks. w/ Bwd.	$\beta(\alpha = 0.2)$				$\beta(\alpha = 0.3)$			
			0.1	0.2	0.3	0.5	0.1	0.2	0.3	0.5
Mean	15	15	27.7	25.3	24.6	23.8	34.2	30.9	29.1	27.7
	15	5	26.8	24.8	24.3	23.1	32.5	29.8	28.0	26.4
	15	0	22.3	20.1	19.1	18.1	26.6	23.9	23.0	20.3
Top-1	15	15	55.5	51.0	47.9	46.9	59.6	55.0	53.7	51.9
	15	5	52.7	49.5	47.1	46.8	57.2	53.0	51.2	50.0
	15	0	35.8	33.7	32.4	31.2	39.6	37.2	36.2	32.7

Table 3. Ablation of the BSSL scanning directions on Breakfast.

MoC	Block	$\beta(\alpha = 0.2)$				$\beta(\alpha = 0.3)$			
		0.1	0.2	0.3	0.5	0.1	0.2	0.3	0.5
Mean	Ours w/o FF	27.6	25.2	24.3	23.7	34.0	30.4	28.8	27.7
	Ours w/ SE [21]	26.5	24.2	23.7	23.1	33.3	30.0	28.2	27.3
	Ours w/ Dil.Conv	26.8	24.0	23.4	22.6	31.6	29.3	27.0	25.9
	Ours	27.7	25.3	24.6	23.8	34.2	30.9	29.1	27.7
Top-1	Ours w/o FF	52.2	48.9	46.7	46.6	54.9	50.3	47.8	42.4
	Ours w/ SE [21]	51.6	48.9	47.0	46.1	57.5	53.1	52.4	50.2
	Ours w/ Dil. Conv	46.6	42.5	41.4	39.7	51.6	48.0	45.4	43.9
	Ours	55.5	51.0	47.9	46.9	59.6	55.0	53.7	51.9

Table 4. Ablation of the MANTA block structure on Breakfast.

MoC	Num. blocks	$\beta(\alpha = 0.2)$				$\beta(\alpha = 0.3)$			
		0.1	0.2	0.3	0.5	0.1	0.2	0.3	0.5
Mean	10	26.6	24.3	23.5	23.1	32.7	29.4	28.1	26.8
	15	27.7	25.3	24.6	23.8	34.2	30.9	29.1	27.7
	20	27.2	24.5	23.4	23.2	32.1	29.3	27.7	26.6
Top-1	10	54.2	49.2	46.7	46.6	57.2	52.5	52.4	49.7
	15	55.5	51.0	47.9	46.9	59.6	55.0	53.7	51.9
	20	54.7	50.5	48.4	47.1	57.8	53.4	52.3	50.5

Table 5. Ablation of the number of MANTA blocks on Breakfast.

Method	Params. (M)	Stages	Blocks	Total Blocks	Inf. Time (sec)
GTDA [55]	3.9	5	9	45	71.8
Transf. (15) [5]	1.2	1	15	15	15.6
Transf. (18) [5]	1.4	1	18	18	18.2
Ours	1.4	1	15	15	1.1

Table 6. Specifications for different models on Breakfast. Inference time is reported for the longest observation and anticipation ratios ($\alpha = 0.3, \beta = 0.5$).

poral receptive field, but unlike SSMS, each element in the sequence has direct access to all others, avoiding the need for information compression at the cost of quadratic complexity. To mitigate the high complexity, window-based transformers [5, 31] limit their computation to a constrained set of values, making the computation sparse and more efficient.

For our experiments, we made use of such a Transformer designed to balance efficiency and performance for long-term dense temporal action segmentation. Specifically, we use the block from [5], which combines local windowed attention to ensure neighbouring consistency with global sparse ‘atrous’ attention to model the sequence’s long-term context. We compare our MANTA block to [5] in Tab. 7, replacing all blocks in our network with theirs. We evaluate two Transformer models with different total block counts to ensure a fair comparison. As shown in Tab. 6, while Transf.(15) with 15 blocks matches the block count in the MANTA architecture, Transf.(18) with 18 blocks matches the parameter count of our proposed network.

While both tested Transformer-based networks outperform the previously proposed GTDA in effectiveness and efficiency, among themselves, Transf.(18) is more effective than Transf.(15), but due to the larger number of layers, it suffers in efficiency. However, both Transformer models fall short compared to our proposed MANTA model. Specifically, our model is $16.5\times$ faster than Transf.(18) and achieves, on average, 1.1% and 2.4% better Mean and Top-1 MoC.

Long-Range Sequence Modelling. In Fig. 5, we fur-

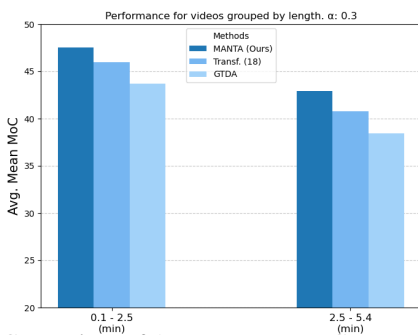


Figure 5. Comparison of Average Mean MoC accuracy for different models on videos grouped by their duration on Breakfast for $\alpha = 0.3$ and $\beta = 0.2$.

MoC	Method	$\beta (\alpha = 0.2)$				$\beta (\alpha = 0.3)$			
		0.1	0.2	0.3	0.5	0.1	0.2	0.3	0.5
Mean	GTDA [55]	24.0	22.0	21.4	20.6	29.1	26.8	25.3	24.2
	Transf. (15) [5]	25.6	23.3	22.5	21.9	30.5	28.1	26.4	25.7
	Transf. (18) [5]	27.3	24.9	24.3	23.3	32.0	29.2	27.5	26.5
	Ours	27.7	25.3	24.6	23.8	34.2	30.9	29.1	27.7
Top-1	GTDA [55]	51.2	47.3	45.6	45.0	54.0	50.4	49.6	47.8
	Transf. (15) [5]	51.2	48.4	45.9	44.0	54.1	51.2	49.3	46.5
	Transf. (18) [5]	52.7	49.1	47.0	45.2	57.2	52.3	50.5	48.2
	Ours	55.5	51.0	47.9	46.9	59.6	55.0	53.7	51.9

Table 7. Ablation of the MANTA block type on Breakfast.

ther examine how our proposed MANTA model performs in comparison to the other tested models across different video lengths. Specifically, we calculate the Average Mean MoC for videos grouped by their duration, *i.e.*, we first compute the Mean MoC for each video individually and then average the results within each length-based group. While MANTA consistently outperforms both Transf.(18) and GTDA on all video lengths, the performance gap increases for longer videos. As discussed in Sec. 3, GTDA encounters difficulties with longer sequences due to the lack of global context caused by the sparse receptive fields of its layers. Despite maintaining a global receptive field across layers, Transf.(18) also yields inferior results compared to our proposed model. We hypothesize that the issue stems from the lack of strong local bias in the Transformer’s temporal updates, which contrasts with the MANTA blocks. The lack of such bias would require the network to learn it from the data, potentially requiring specifically tailored optimization procedures and/or larger training sets.

5. Conclusion

In this work, we proposed a novel MANTA model for stochastic long-term dense anticipation. While prior work aimed to model framewise past and future actions simultaneously, its performance was limited by the sparse receptive fields of its temporal modelling layers, resulting in redundant parameters and increased computational costs. To address these challenges, we introduced the MANTA generator network, which maintains a locally-aware global receptive field throughout the network, eliminating the need for multi-stage architectures and reducing both memory and computational requirements. Additionally, our model can adaptively process sequences with distinct observed and masked regions even for very long sequences. Experimental results on three datasets demonstrate that MANTA achieves state-of-the-art performance while achieving significant speed improvements.

References

- [1] Y. Abu Farha, Q. Ke, B. Schiele, and J. Gall. Long-term anticipation of activities with cycle consistency. In *DAGM German Conference on Pattern Recognition (GCPR)*, 2020.

- [2] Y. Abu Farha, A. Richard, and J. Gall. When will you do what?-Anticipating temporal occurrences of activities. In *IEEE Conference on Computer Vision and Pattern Recognition (CVPR)*, 2018.
- [3] K. Ashutosh, R. Girdhar, L. Torresani, and K. Grauman. Hierarchy: Learning hierarchical video-language embeddings. In *IEEE Conference on Computer Vision and Pattern Recognition (CVPR)*, 2023.
- [4] Jimmy Lei Ba. Layer normalization. *arXiv preprint arXiv:1607.06450*, 2016.
- [5] Emad Bahrami, Gianpiero Francesca, and Juergen Gall. How much temporal long-term context is needed for action segmentation? In *IEEE International Conference on Computer Vision (ICCV)*, 2023.
- [6] S. Das and M. S. Ryoo. Video + clip baseline for ego4d long-term action anticipation. *ArXiv*, 2022.
- [7] Y. Farha and J. Gall. Uncertainty-aware anticipation of activities. In *IEEE International Conference on Computer Vision Workshop (ICCVW)*, 2019.
- [8] A. Furnari and G. M. Farinella. Rolling-unrolling lstms for action anticipation from first-person video. *IEEE Transactions on Pattern Analysis and Machine Intelligence (TPAMI)*, 2020.
- [9] Harshayu Girase, Nakul Agarwal, Chiho Choi, and Kartikeya Mangalam. Latency matters: Real-time action forecasting transformer. In *IEEE/CVF Conference on Computer Vision and Pattern Recognition (CVPR)*, 2023.
- [10] R. Girdhar and K. Grauman. Anticipative Video Transformer. In *IEEE International Conference on Computer Vision (ICCV)*, 2021.
- [11] D. Gong, J. Lee, M. Kim, S.J. Ha, and M. Cho. Future transformer for long-term action anticipation. In *IEEE Conference on Computer Vision and Pattern Recognition (CVPR)*, 2022.
- [12] K. Grauman, A. Westbury, and et al. Ego4d: Around the world in 3,000 hours of egocentric video. *IEEE Conference on Computer Vision and Pattern Recognition (CVPR)*, 2022.
- [13] Albert Gu and Tri Dao. Mamba: Linear-time sequence modeling with selective state spaces. *arXiv preprint arXiv:2312.00752*, 2023.
- [14] Albert Gu, Karan Goel, and Christopher Re. Efficiently modeling long sequences with structured state spaces. In *International Conference on Learning Representations*, 2022.
- [15] Albert Gu, Isys Johnson, Karan Goel, Khaled Saab, Tri Dao, Atri Rudra, and Christopher Ré. Combining recurrent, convolutional, and continuous-time models with linear state space layers. In M. Ranzato, A. Beygelzimer, Y. Dauphin, P.S. Liang, and J. Wortman Vaughan, editors, *Advances in Neural Information Processing Systems*, 2021.
- [16] Hongji Guo, Nakul Agarwal, Shao-Yuan Lo, Kwonjoon Lee, and Qiang Ji. Uncertainty-aware action decoupling transformer for action anticipation. In *IEEE/CVF Conference on Computer Vision and Pattern Recognition (CVPR)*, 2024.
- [17] Hang Guo, Jinmin Li, Tao Dai, Zhihao Ouyang, Xudong Ren, and Shu-Tao Xia. Mambair: A simple baseline for image restoration with state-space model. In *European Conference on Computer Vision*, 2025.
- [18] Dongchen Han, Ziyi Wang, Zhuofan Xia, Yizeng Han, Yifan Pu, Chunjiang Ge, Jun Song, Shiji Song, Bo Zheng, and Gao Huang. Demystify mamba in vision: A linear attention perspective. *arXiv preprint arXiv:2405.16605*, 2024.
- [19] Dan Hendrycks and Kevin Gimpel. Gaussian error linear units (gelus). *arXiv: Learning*, 2016.
- [20] Jonathan Ho, Ajay Jain, and Pieter Abbeel. Denoising diffusion probabilistic models. *Advances in Neural Information Processing Systems (NeurIPS)*, 2020.
- [21] Jie Hu, Li Shen, Samuel Albanie, Gang Sun, and Enhua Wu. Squeeze-and-excitation networks. *IEEE Conference on Computer Vision and Pattern Recognition (CVPR)*, 2018.
- [22] Vincent Tao Hu, Stefan Andreas Baumann, Ming Gui, Olga Grebenkova, Pingchuan Ma, Johannes Fischer, and Björn Ommer. Zigma: A dit-style zigzag mamba diffusion model. In *ECCV*, 2024.
- [23] Q. Ke, M. Fritz, and B. Schiele. Time-conditioned action anticipation in one shot. In *IEEE Conference on Computer Vision and Pattern Recognition (CVPR)*, 2019.
- [24] Hilde Kuehne, Ali Arslan, and Thomas Serre. The language of actions: Recovering the syntax and semantics of goal-directed human activities. In *IEEE Conference on Computer Vision and Pattern Recognition (CVPR)*, 2014.
- [25] Kunchang Li, Xinhao Li, Yi Wang, Yanan He, Yali Wang, Limin Wang, and Yu Qiao. Videomamba: State space model for efficient video understanding. In *European Conference on Computer Vision*, 2025.
- [26] Shufan Li, Harkanwar Singh, and Aditya Grover. Mamband: Selective state space modeling for multi-dimensional data. In *European Conference on Computer Vision*, 2025.
- [27] Dingkan Liang, Xin Zhou, Wei Xu, Xingkui Zhu, Zhikang Zou, Xiaoqing Ye, Xiao Tan, and Xiang Bai. Pointmamba: A simple state space model for point cloud analysis. In *Advances in Neural Information Processing Systems*, 2024.
- [28] J. Lin, C. Gan, K. Wang, and S. Han. Tsm: Temporal shift module for efficient and scalable video understanding on edge devices. *IEEE Transactions on Pattern Analysis and Machine Intelligence (TPAMI)*, 2020.
- [29] Miao Liu, Siyu Tang, Yin Li, and James M Rehg. Forecasting human-object interaction: joint prediction of motor attention and actions in first person video. In *European Conference on Computer Vision (ECCV)*, 2020.
- [30] Yue Liu, Yunjie Tian, Yuzhong Zhao, Hongtian Yu, Lingxi Xie, Yaowei Wang, Qixiang Ye, and Yunfan Liu. Vmamba: Visual state space model. *arXiv preprint arXiv:2401.10166*, 2024.
- [31] Ze Liu, Yutong Lin, Yue Cao, Han Hu, Yixuan Wei, Zheng Zhang, Stephen Lin, and Baining Guo. Swin transformer: Hierarchical vision transformer using shifted windows. In *Proceedings of the IEEE/CVF International Conference on Computer Vision (ICCV)*, 2021.
- [32] Jun Ma, Feifei Li, and Bo Wang. U-mamba: Enhancing long-range dependency for biomedical image segmentation. *arXiv preprint arXiv:2401.04722*, 2024.
- [33] E.V. Mascaró, H. Ahn, and D. Lee. Intention-conditioned long-term human egocentric action anticipation. In *IEEE Winter Conference on Applications of Computer Vision (WACV)*, 2023.

- [34] Himangi Mittal, Nakul Agarwal, Shao-Yuan Lo, and Kwong Lee. Can't make an omelette without breaking some eggs: Plausible action anticipation using large video-language models. In *IEEE/CVF Conference on Computer Vision and Pattern Recognition (CVPR)*, 2024.
- [35] Shentong Mo and Yapeng Tian. Scaling diffusion mamba with bidirectional ssms for efficient image and video generation. *arXiv preprint arXiv:2405.15881*, 2024.
- [36] T. Nagarajan, Y. Li, C. Feichtenhofer, and K. Grauman. Ego-topo: Environment affordances from egocentric video. In *IEEE Conference on Computer Vision and Pattern Recognition (CVPR)*, 2020.
- [37] M. Nawhal, A. A. Jyothi, and G. Mori. Rethinking learning approaches for long-term action anticipation. In *European Conference on Computer Vision (ECCV)*, 2022.
- [38] Prajit Ramachandran, Barret Zoph, and Quoc Le. Swish: a self-gated activation function. *arXiv: Learning*, 2017.
- [39] Aditya Ramesh, Prafulla Dhariwal, Alex Nichol, Casey Chu, and Mark Chen. Hierarchical text-conditional image generation with clip latents. *ArXiv preprint*, 2022.
- [40] Debaditya Roy, Ramanathan Rajendiran, and Basura Fernando. Interaction region visual transformer for egocentric action anticipation. In *IEEE/CVF Winter Conference on Applications of Computer Vision (WACV)*, 2024.
- [41] Jiacheng Ruan and Suncheng Xiang. Vm-unet: Vision mamba unet for medical image segmentation. *arXiv preprint arXiv:2402.02491*, 2024.
- [42] F. Sener, D. Chatterjee, D. Shelepov, K. He, D. Singhania, R. Wang, and A. Yao. Assembly101: A large-scale multi-view video dataset for understanding procedural activities. *IEEE Conference on Computer Vision and Pattern Recognition (CVPR)*, 2022.
- [43] Fadime Sener, Dipika Singhania, and Angela Yao. Temporal aggregate representations for long-range video understanding. In *European Conference on Computer Vision (ECCV)*, 2020.
- [44] Yuheng Shi, Mingjing Dong, and Chang Xu. Multi-scale vmamba: Hierarchy in hierarchy visual state space model. *arXiv preprint arXiv:2405.14174*, 2024.
- [45] Jimmy T.H. Smith, Andrew Warrington, and Scott Linderman. Simplified state space layers for sequence modeling. In *The Eleventh International Conference on Learning Representations*, 2023.
- [46] Jascha Sohl-Dickstein, Eric Weiss, Niru Maheswaranathan, and Surya Ganguli. Deep unsupervised learning using nonequilibrium thermodynamics. In *International Conference on Machine Learning (ICML)*, 2015.
- [47] Jiaming Song, Chenlin Meng, and Stefano Ermon. Denoising diffusion implicit models. In *International Conference on Learning Representations*, 2021.
- [48] Yang Song and Stefano Ermon. Generative modeling by estimating gradients of the data distribution. *Advances in Neural Information Processing Systems (NeurIPS)*, 2019.
- [49] Yang Song, Jascha Sohl-Dickstein, Diederik P Kingma, Abhishek Kumar, Stefano Ermon, and Ben Poole. Score-based generative modeling through stochastic differential equations. In *International Conference on Learning Representations (ICLR)*, 2021.
- [50] Sebastian Stein and Stephen J. McKenna. Combining embedded accelerometers with computer vision for recognizing food preparation activities. *ACM international joint conference on Pervasive and ubiquitous computing*, 2013.
- [51] A. Vaswani, N. Shazeer, N. Parmar, J. Uszkoreit, L. Jones, A. N. Gomez, L. Kaiser, and I. Polosukhin. Attention is all you need. In *Advances in Neural Information Processing Systems (NeurIPS)*, 2017.
- [52] Jue Wang, Wentao Zhu, Pichao Wang, Xiang Yu, Linda Liu, Mohamed Omar, and Raffay Hamid. Selective structured state-spaces for long-form video understanding. In *Proceedings of the IEEE/CVF Conference on Computer Vision and Pattern Recognition*, 2023.
- [53] Zhaohu Xing, Tian Ye, Yijun Yang, Guang Liu, and Lei Zhu. Segmamba: Long-range sequential modeling mamba for 3d medical image segmentation. In *International Conference on Medical Image Computing and Computer-Assisted Intervention*, 2024.
- [54] Jing Nathan Yan, Jiatao Gu, and Alexander M Rush. Diffusion models without attention. In *Proceedings of the IEEE/CVF Conference on Computer Vision and Pattern Recognition*, pages 8239–8249, 2024.
- [55] Olga Zatsarynna, Emad Bahrami, Yazan Abu Farha, Gianpiero Francesca, and Juergen Gall. Gated temporal diffusion for stochastic long-term dense anticipation. *European Conference on Computer Vision (ECCV)*, 2024.
- [56] O. Zatsarynna, Y. Farha, and J. Gall. Multi-modal temporal convolutional network for anticipating actions in egocentric videos. In *IEEE Conference on Computer Vision and Pattern Recognition Workshop (CVPRW)*, 2021.
- [57] Olga Zatsarynna, Yazan Abu Farha, and Juergen Gall. Self-supervised learning for unintentional action prediction. In *DAGM German Conference on Pattern Recognition (GCPR)*, 2022.
- [58] O. Zatsarynna and J. Gall. Action anticipation with goal consistency. In *IEEE International Conference on Image Processing (ICIP)*, 2023.
- [59] Zeyu Zhang, Akide Liu, Ian Reid, Richard Hartley, Bohan Zhuang, and Hao Tang. Motion mamba: Efficient and long sequence motion generation. In *European Conference on Computer Vision*, 2025.
- [60] H. Zhao and R. P. Wildes. On diverse asynchronous activity anticipation. In *European Conference on Computer Vision (ECCV)*, 2020.
- [61] Qi Zhao, Ce Zhang, Shijie Wang, Changcheng Fu, Nakul Agarwal, Kwong Lee, and Chen Sun. Antgpt: Can large language models help long-term action anticipation from videos? *International Conference on Learning Representations (ICLR)*, 2024.
- [62] Y. Zhao and P. Krähenbühl. Real-time online video detection with temporal smoothing transformers. In *European Conference on Computer Vision (ECCV)*, 2022.
- [63] Zeyun Zhong, David Schneider, Michael Voit, Rainer Stiefelhagen, and Jürgen Beyerer. Anticipative feature fusion transformer for multi-modal action anticipation. In *IEEE Winter Conference on Applications of Computer Vision (WACV)*, 2023.

- [64] Zeyun Zhong, Chengzhi Wu, Manuel Martin, Michael Voit, Juergen Gall, and Jürgen Beyerer. Diffant: Diffusion models for action anticipation. *ArXiv*, 2023.
- [65] Lianghui Zhu, Bencheng Liao, Qian Zhang, Xinlong Wang, Wenyu Liu, and Xinggang Wang. Vision mamba: Efficient visual representation learning with bidirectional state space model. *arXiv preprint arXiv:2401.09417*, 2024.